Ain Shams Engineering Journal 15 (2024) 102393

Contents lists available at ScienceDirect

Ain Shams Engineering Journal

journal homepage: www.sciencedirect.com

FEM-based analysis of rotor cage material and slot geometry on double air gap axial flux induction motors

Mustafa Özsoy [a,*], Orhan Kaplan [b], Mehmet Akar [c]

[a] Electrical and Electronics Engineering Department, Gazi University Graduate School of Natural and Applied Sciences, 06500 Beşevler/Ankara, Turkey
[b] Faculty of Technology, Department of Electrical and Electronics Engineering, Gazi University, 06500 Beşevler/Ankara, Turkey
[c] Faculty of Engineering and Architecture Sciences, Department of Electric Electronical Engineering, Tokat Gaziosmanpasa University, 60150 Tokat, Turkey

ARTICLE INFO

Keywords:
Axial flux
Induction motor
Double gap
Rotor slot geometry
Rotor shape
Cage material

ABSTRACT

The aim of this study is to research the effect of rotor slots geometry and squirrel cage material on motor performance in Axial Flux Induction Motors (AFIM) by analysing with finite element method. It is aimed to present a motor design with higher efficiency and low torque ripple, especially for use in electric vehicles. This study aims to design a double stator AFIM with a rated power of 50 kW. Aluminium, and copper cage motors with same stator structure but with 6 different rotor slots geometries are compared. Saturation of cores and current density of coils are considered as limit parameters. Using copper bars with rotor slot1, 92.12% efficiency was obtained with 5.77% torque ripple.

1. Introduction

Induction motors are more widely used than other members of the electric motor family. The main reasons for their widespread use are that they are easy to produce, have a simple and robust structure and low maintenance costs. Since induction motors do not contain magnets, they always maintain their advantages in terms of cost. The fact that magnet costs have become an important component in motor cost has caused motor manufacturers to focus on magnetless designs. For this reason, in addition to the advantages mentioned, induction motors have regained the attention of researchers despite their low starting torque, high starting current, low power factor at low slip and inefficiency compared to alternatives. These disadvantages can be partially overcome by developing motor control methods. Induction motors have become widely used in variable speed applications such as electric vehicles with the developments in speed control methods. Induction motors, which have the potential to be used in current applications such as electric vehicles with their established technology, encourage researchers to work on this subject.

Thanks to the developments in production technologies, complex designs have become possible. In addition, it has become necessary to produce electric motors in lower volumes with high torque density. One of the motors that best meets this need is the axial flux (AF) motors[1]. AF motors have higher torque density in the same volume compared to radial flux alternatives. Since the magnetic flux is distributed axially in AF motors, the motor diameter is larger than the axial length [2]. This provides a longer force arm and thus high torque is obtained. The construction of AF motors is more complex than conventional radial flux motors. Due to the inside to outside expansion of the diameter, the magnetic flux path is shortest at the inner diameter and longest at the outer diameter [3]. This results in narrower tooth thickness at the inner diameter and wider teeth at the outer diameter. Different tooth thicknesses result in teeth closer to saturation in the inner diameter and lower flux density in the outer diameter. For this reason, AF motors are problems that should be handled in three dimensions (3D). Simulations with 3D models cause long analysis times and extra processor load [4]. This causes difficulties for the designers. The extra load of the design process due to the 3D model can be significantly reduced by using two-dimensional (2D) linear equivalent models obtained by using the dimensions of the AF motors with average diameter values [5].

Axial Flux Induction Motors (AFIM) provide advantages over radial flux alternatives, especially in terms of torque density. However, since they need to be produced in larger diameters at high powers, it causes an increase in the axial pulling force between the rotor and stator. The increased axial force causes a balance problem. This problem can be minimized by using double air gap topologies[6]. In double air gap topologies, a more balanced force distribution is obtained since a symmetrical pulling force is formed. In addition, for double air gap

* Corresponding author.
E-mail address: mustafa.ozsoy@gop.edu.tr (M. Özsoy).

https://doi.org/10.1016/j.asej.2023.102393
Received 14 November 2022; Received in revised form 12 April 2023; Accepted 15 July 2023
Available online 26 July 2023

topologies, in the rotor yoke between the air gaps, topologies that allow the magnetic flux to pass directly from the rotor core to the stator core or to complete the flux path separately from the stator cores can be obtained. This enables different slot designs in the rotor slot structure compared to conventional radial flux induction motors. Among double air gap topologies, double rotor AF motors have been reported to provide higher torque density at high current density levels [7]. In double air gap designs, coreless designs also become possible[8]. In addition, it has been reported that yokeless designs contribute to motor efficiency as core losses affecting motor efficiency are reduced [9]. The fact that the stator magnetic flux completes its flux path without splitting on the rotor core causes the rotor core to consist of as many parts as the number of slots. In the production phase, this obstacle can be overcome by using a solid rotor core. However, in this case, the laminations of the rotor core, which must be positioned radially, cannot be obtained. The production of the rotor core in this way will have a negative effect on the motor efficiency. With the developments in additive manufacturing techniques, it has become possible to produce the rotor core in laminated form [9]. In Fig. 1, the components of an AFIM with double stator NS topology are shown using the ¼ model.

Aluminium (Al) is generally preferred as rotor bar material in induction motors. Although mostly cast rotors are produced from Al, with the developing technology, cast rotors can also be produced by copper (Cu) injection method. Special Al and Cu alloys are also used especially for motors operating at high slip, which are in class D in NEMA classification [10].

Cu squirrel cages have lower resistance than Al cages and therefore provide an advantage in efficiency. However, Al is preferred because it can be shaped more easily than Cu and is a relatively inexpensive material. For example, high resistance Cu alloy material is generally preferred in NEMA C and D class motors[10].

The geometrical design of the rotor slot is an important stage in determining the motor performance. Because the shape of the torque speed curve is largely determined at this step. Typically, rotor slots have trapezoidal, rectangular, round or Boucherot geometries[11].

In AFIM, as in radial flux motors, rotor bars with low skin effect result in low starting torque and high efficiency. The opposite effect is observed with high skin effect. Especially during acceleration, the skin effect causes the rotor bar current to concentrate on the upper part of the bar, which plays an active role in determining the starting torque and starting current. When the motor is at standstill, the skin effect forces the current to flow through the top of the bar. This upper part of the bars of the squirrel cage is designed to have high resistance and reactance. With high resistance and reactance, low instantaneous current and high torque are obtained.

For Double Stator Axial Flux Induction Motors (DS-AFIM), with double cage structures and deep slots in rotor geometric shapes, it is aimed to obtain high efficiency, high starting torque, low starting current and low nominal slip at the same. For this purpose, it is possible to obtain a variable resistance for transient and steady state operation by changing the rotor slot structure[12]. At low speeds, high bar resistance increases the starting torque. However, at high speeds, high bar resistance negatively affects the efficiency[12]. The motor load will increase in a proportional increase with the slip. This means an increase in rotor frequency. Since leakage reactance will also increase at high rotor frequency, negative effects on motor performance are observed[12]. When the effect of rotor shape on the torque speed curve is analysed, it is shown that short and wide bars provide higher initial torque and higher power factor, while deep and wide bars provide an advantage in efficiency[13]. Round slots have been reported to provide better acoustic performance than rectangular slots in the same slot area[14].

Deep slot motors have a higher leakage reactance. This means low starting current. Open slots cause high air gap concentration, which means low power factor (pf), high air gap reluctance and high ripple losses in the teeth, as well as noise and vibration. Open slots also require higher magnetizing current. However, the leakage reactance is lower in open slot motors. Motor torque at full load and pull out torque are inversely proportional to motor leakage reactance. In other words, open slot motors have high breakdown torque and high pull out torque at the expense of low pf. In semi-closed slot motors, the width of the slot opening is narrower than open slot motors. In this way, the air gap characteristics are better than the open slot. The advantages are lower air gap concentration factor, lower magnetization current, low tooth ripple loss and low noise. It is generally the preferred slot type in induction motors. The disadvantage is that the leakage flux and leakage reactance are slightly higher. In these motors, pf is better, but breakdown torque and pull-up torque are lower than open slot.

High leakage reactance in closed slots limits the starting current. The disadvantage is that high leakage reactance reduces the overload capacity. Semi-closed slots have better overload capacity. Deep conical (deep trapezoidal) shaped slots are usually used in combination with a round upper slot part. This is because the high leakage reactance in the rectangular region at the bottom of the slot, forces most of the current to flow through the round upper region at start-up. This non-uniform current distribution increases the effective rotor resistance, thus increasing the starting torque. Tooth pulsation losses decrease as the number of slots increases. The slot openings increase the air gap reluctance and the air gap reluctance changes according to the slot position. The changing reluctance in the air gap causes tooth pulsation loss and noise. Tooth pulsation loss and noise can be minimized with a high number of slots or semi-closed slots with narrow openings. After these processes, optimization can be applied for both stator and rotor slots and better motor performances can be obtained with more precise measurements[15]. In addition, the optimization process should be evaluated in terms of cost instead of being considered only in terms of motor performance[16].

In this study, DS-AFIM designs with different rotor slot geometries have been made for use as traction motors in electric vehicles with a nominal power of 50 kW and a maximum power of 75 kW, taking into account the effects mentioned in the rotor slot design. In the designed motors, double stator NS topology is used to complete the magnetic circuit between the two stators without separating the flux from the rotor core. Double stator topology was preferred due to the ease of integration of the cooling jacket into the motor body. In traditional manufacturing methods, which are more common in today's conditions, it is very difficult to produce the rotor core in pieces from laminated

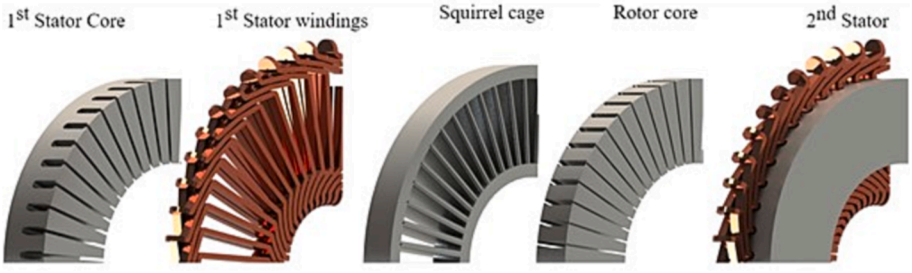

Fig. 1. 3D ¼ model of double stator AFIM.

steel. For this reason, the rotor core is modelled as solid steel. Further studies will be carried out to produce the rotor core with additive manufacturing method and soft magnetic material. Since the design purpose of the motor is to be used in electric vehicles, better starting torque and high efficiency at nominal operation are targeted. For this reason, double chamber slots were also analysed in the rotor geometries. In order to obtain high efficiency, Cu is preferred in rotor bars. In order to compare the effect of Cu used in the squirrel cage, more commonly used Al cage motor analyses were also performed in the same rotor slot geometry. To fairly compare the effects of the materials and slot geometries, the stator parameters were selected at the same values for each motor. The comparisons are based on the results of analyses using the Finite Element Method (FEM) on 2D linear models of AFIMs. Since the motors will be used in variable speed applications, the results are expressed in speed dependent torque, current, efficiency and power graphs. To obtain these graphs, 2D linear models of the motors were analysed parametrically. In this study, AFIM with high torque density, surpassing that of radial flux counterparts, is developed for utilization as a traction motor in electric vehicles. To circumvent the need for magnets, which are classified as rare earth elements, and to capitalize on the expertise garnered from radial flux designs, an induction motor is chosen. Double stator topology is used to overcome the unbalanced axial force, which is an important drawback of axial flux motors. The effects of various rotor geometries in AFIM designs, where research is less frequent compared to radial flux alternatives, are investigated by examining six different rotor slot geometries. In addition, expectation for high efficiency motors in electric vehicles has been met by using copper squirrel cage. The effect of squirrel cage material and rotor slot geometry at different slip values is presented through speed-dependent torque, current, efficiency and power graphs. Each motor is analysed using 2D linear equivalent models instead of using complex and time-consuming 3D models. The comparison of AFIMs in terms of both slot geometry and squirrel cage material using linear equivalent models is expected to provide useful guidance for researchers.

2. Axial flux induction motor design

Since the motor proposed in this study will be used as an electric vehicle drive motor, the motor requirements and related dimensioning have been determined appropriately[14]. The motor design criteria are given in Table 1. In a study examining the torque and current ripples due to the number of poles, number of stator slots and number of bars in a radial-flux induction motor, some preliminary information is given to the designers [17]. Therefore, for an 8-pole motor, stator slot combinations are proposed as 24,48 and 72 when the bars are not skewed. The number of rotor slots is proposed as 22,26,34 for 24 stator slots, 30,50,54,58 for 48 stator slots, 42,50,58 and 82 for 72 stator slots. Thus, as one of the combinations in which minimum torque and current ripple is obtained, 8 pole 48/54 slot number is preferred.

Table 1
Motor design parameters.

Parameter	Value
Pole number	8
Stator slot number	48
Rotor slot number	54
Outer diameter (mm)	245
Inner diameter (mm)	150
Stator thickness (mm)	40
Rotor thickness (mm)	30
Air gap (mm)	0.7
Stator windings	Copper
Rotor material (Solid)	JFE_Steel_50JN1000
Stator material (Laminated)	JFE_Steel_35JN270
Rated frequency (Hz)	266.67
Rated Speed (rpm)	4000
Lamination stacking factor	0.97
Bss0 – Stator slot opening width (mm)	2.5
Bss1 – Stator slot wedge maximum width (mm)	6.5
Bss2 - Stator slot body bottom width (mm)	6.5
Hss0 – Stator slot opening height (mm)	1.5
Hss1 – Stator slot wedge height (mm)	1.5
Hss2 – Stator slot body height (mm)	18.75

In AFIM design, sizing equations are a practical method for determining the dimensions of the designed motor, such as slot dimensions, according to the air gap flux density. The air gap flux density is calculated according to the equation given in Equation (1)[18].

$$\varphi_{ax} = B_{max}\sin\left(\frac{p}{2}\theta - \omega_s t\right) \tag{1}$$

Here φ_{ax} is the axial rotary magnetic flux in the air gap, B_{max} is the maximum flux density in the air gap, p is the number of poles, θ s the rotary mechanical angle in the air gap and, ω_s is the angular velocity. The total magnetic flux density is obtained according to equation (1) and then divided by the number of poles to obtain the magnetic flux per pole [18].

$$\varphi_p = \frac{\left(D_{out}^2 - D_{in}^2\right)B_{max}}{2p} \tag{2}$$

$$\varphi_{rt} = \varphi_p \tag{3}$$

$$\varphi_{ry} = \frac{\pi\left(D_{out}^2 - D_{in}^2\right)B_{max}}{4Q_r} \tag{4}$$

Magnetic flux per pole φ_p calculated according to Equation (2). Here D_{out} motor outer diameter, D_{in} refers to the inner diameter of the motor. In Equation (3) and Equation (4) φ_{rt} and φ_{ry} refers to the magnetic flux in the rotor teeth and rotor yoke respectively. Q_r is the number of rotor slots. According to the determined magnetic flux density limit values, the axial length of the rotor yoke is determined according to Equation (5)[18].

$$l_{ry} = \frac{(D_{out} + D_{in})B_{max}}{pB_{r,y}C_{rlam}} \tag{5}$$

In Equation (5) $B_{r,y}$ and C_{lam} represent the maximum flux density at the rotor yoke and the rotor stack factor, respectively. Depending on the number of rotor slots and slot dimensions, the magnetic flux density in the rotor teeth will change. Moreover, due to the geometry of axial flux motors, the motor diameter increases from inside to outside. Since the slot dimensions are constant, the rotor teeth will have the narrowest tooth thickness at the inner diameter and the widest tooth thickness at the outer diameter. Therefore, the calculation of the tooth thickness should be based on the inner diameter value. When the rotor geometry changes, the narrowest region should be determined by considering these calculations. Thus, the rotor tooth width is determined according to Equation (6). In Equation (6) $B_{r,t}$ refers to the maximum flux density in the rotor teeth[18].

$$w_{r,t} = \frac{\pi B_{max} D_{in}}{Q_r B_{r,t} C_{rlam}} \tag{6}$$

Rotor slot width and height are calculated according to Equation (7) and Equation (8), respectively. In Equation (7) τ_r refers to the slot spacing. In Equation (8) i_r refers to the rotor bar currents magnitude, J_r refers to maximum current density of rotor bar, $C_{r,fill}$ refers to rotor slot fill factor[18].

$$w_{r,sl} = \tau_r - w_{r,t} \tag{7}$$

$$h_{r,sl} = \frac{i_r}{J_r C_{r,fill} w_{r,sl}} \tag{8}$$

3. Linear model of axial flux induction motor

The final design of AFIM is a problem that must be addressed in 3D.

However, designers may want to implement many different alternatives in their designs before the final model. This is quite time consuming with 3D models [19]. For this reason, it is one of the preferred methods to analyse AFIMs via 2D linear models, where faster results can be obtained [18]. In fact, there are studies on linear modelling of not only AFIMs but also different AF Motors [20]. In 2D designs, especially effects that can only be measured with 3D models, such as winding end effects, can be analysed with acceptable accuracy in 2D models[4]. In 2D Linear models of AFIMs based on the average diameter, the accuracy of the solution can be increased in a similar way to the average diameter, but with a larger number of slices of different diameter values [2122]. In all cases, 2D models are advantageous in terms of analysis time. But although most of the intermediate processes are performed with 2D models, the 3D final model is taken into consideration by the designers before prototyping. In the AFIM 2D model, a 2D Linear model is used, which is obtained according to the slot and tooth dimensions of the average value of the inner and outer diameter. Since the rotor and stator are positioned parallel to each other in axial flux motors, the 2D linear model is obtained by unwrapping the section taken from the average diameter value. The area A_c of the circular section from the 3D model and the rectangular area A_r of the 2D linear model are equal. A_c and A_r are calculated according to Equation (9) and Equation (10) [23].

$$A_c = \frac{\pi}{2p}\left(D_o^2 - D_i^2\right) \tag{9}$$

$$A_r = \frac{\left(D_o^2 - D_i^2\right)}{2} \bullet \frac{\pi(D_o + D_i)}{p} = \frac{\pi}{2p}\left(D_o^2 - D_i^2\right) \tag{10}$$

The time dependent torque graph of an AFIM analysed with a 2D Linear model obtained according to the design parameters taken from the average diameter and a motor analysed using the 3D model are shown in Fig. 2. In these analyses, the slot defined as Slot1 in Fig. 3 was analysed with Cu squirrel cage at a nominal power of 50 kW. Therefore, the average moment values at steady state were obtained as 123.84 Nm and 120.88 Nm for 3D and Linear models, respectively, while the currents were obtained as 205.72 A_{rms} and 196.05 A_{rms}. When the 3D model is taken as reference, it means that results are obtained with a relative error of 2.39%.

Working with a 2D model instead of a 3D model has some disadvantages in terms of FEM. The main one is that motor components such as end windings and squirrel rings are expressed as approximate equivalent resistances. In addition, the skew operation can be defined as an external function rather than its geometric shape through the 2D model. In 2D model, the active components of the motor are also considered with the FEM method. The 3rd dimension (z-axis) is expressed by the active radius value (R_a) of the stator. R_a is calculated according to Equation (11)[23]. In the 2D linear motor model, the rotor motion must be defined as displacement since there is no part rotating around a center. Again, because of the linear model, since there is no angular motion, there is no torque produced. Instead, a force is obtained in the linear plane. The obtained force is multiplied by the radius value and the torque value obtained from the 3D model is expressed.

$$R_a = \frac{D_o - D_i}{2} \tag{11}$$

In the FEM analyses performed in this study, 2D linear models of the motors were used. Fig. 3a shows the 2D linear DS-AFIM model using rotor slot number 1. Fig. 3b shows the rotor slot used with the same stator slot and winding structure but different slot geometry.

Factors determining motor performance such as motor starting torque, power factor and efficiency are taken into consideration in the determined rotor slot geometries. Deep and wide slots are proposed to obtain better starting torque and power factor [4]. Cooling is an important factor for more efficient operation in electric motors[24]. Since it is used more and more widely in electric vehicles, a liquid-cooled design is planned. According to this, the current density in the stator windings should be in the range of 6–14 A/mm^2 in designs where the stator windings are cooled with a liquid-cooled stator jacket[25]. In peak operation, it can exceed 25 A/mm^2[2627].

4. Effect of rotor bar material and slot geometry

Speed dependent graphs are good indicators in the evaluation of motor performance. Because as the load on the rotor shaft increases, the rotation speed will decrease and accordingly the slip will increase. The results obtained depending on the slip value in grid-fed AFIMs give information about the starting torque, pull-up torque, breakdown torque and nominal operation of the motor. When this slip and skin effect are

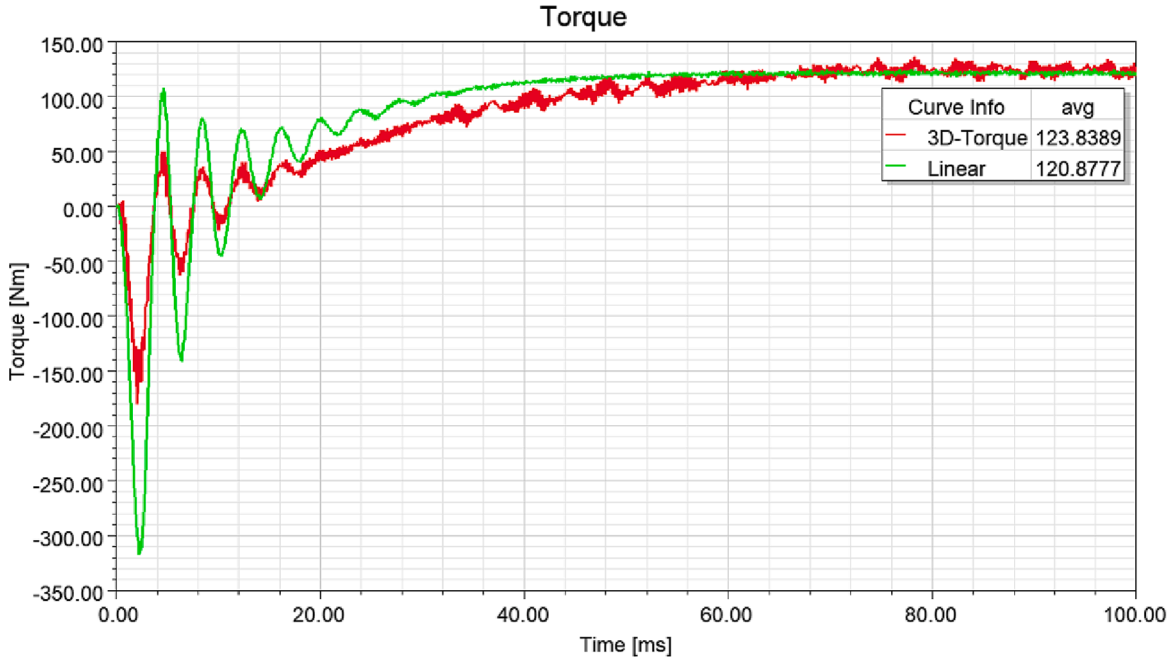

Fig. 2. Torque-time graph of 3D and 2D Linear models.

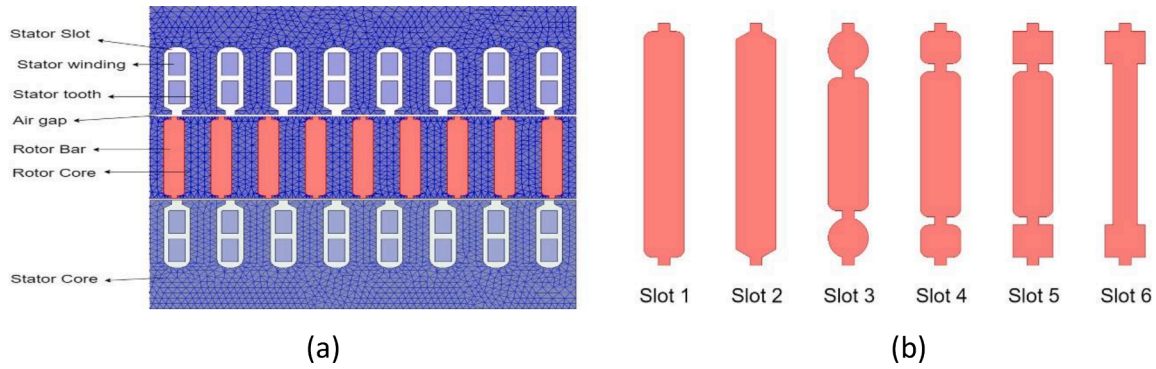

Fig. 3. 2D Linear FEM Model of 48 Stator 54 Rotor Slot AFIM (a) 1/6 Model of 2D Linear Model belongs to Slot1 (b) All slots used in designs.

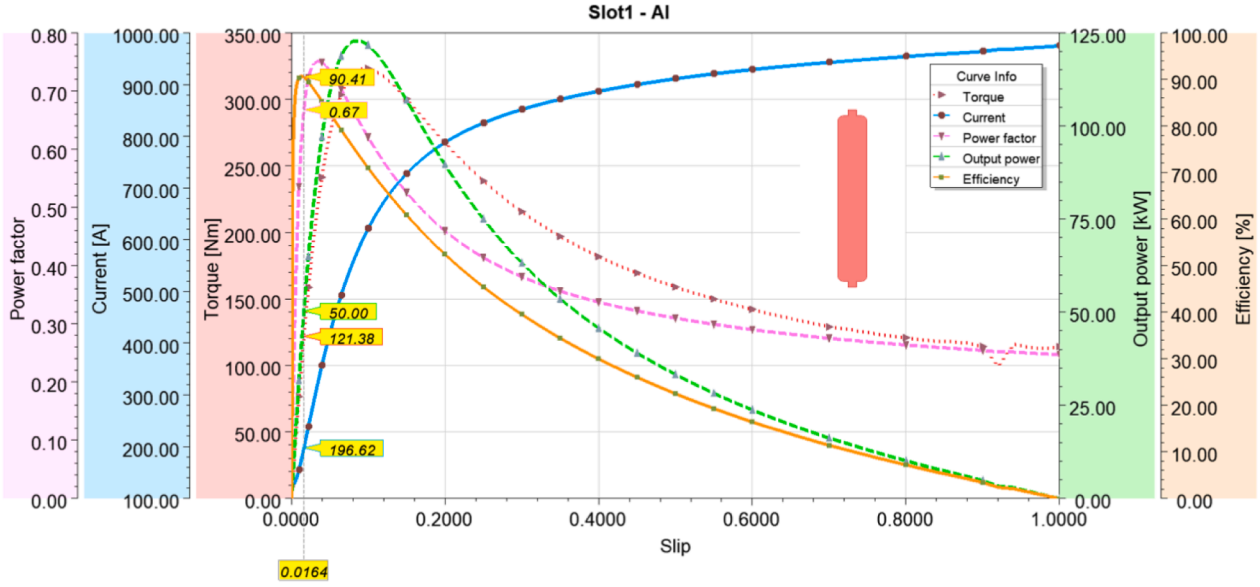

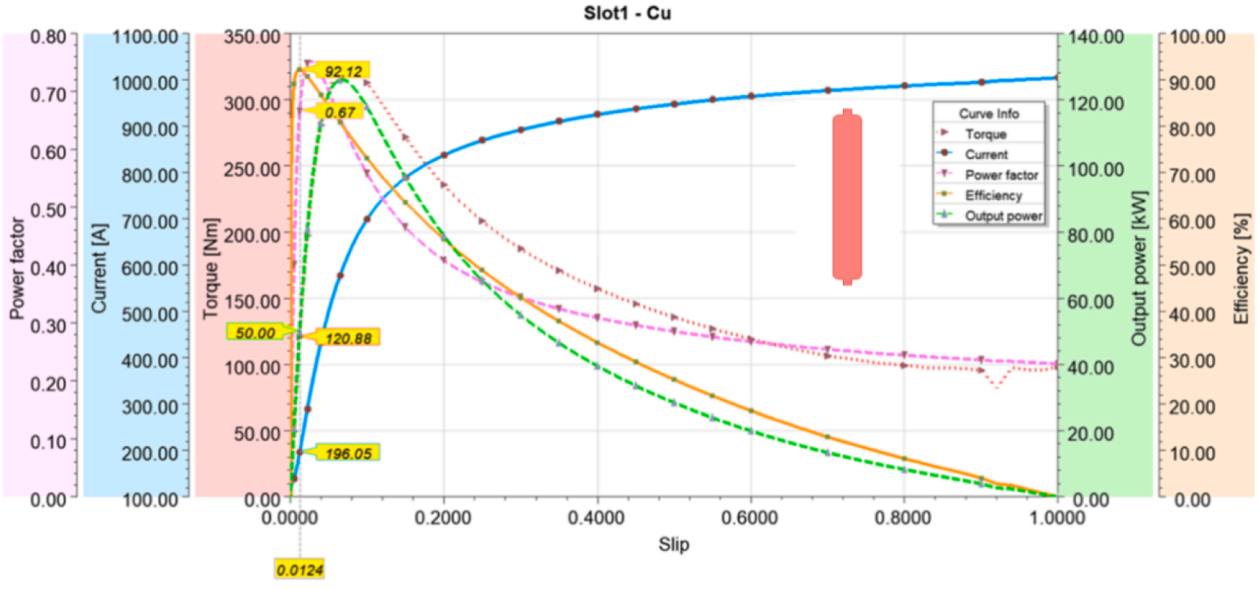

Fig. 4. Slot1 slip dependent performance curves.

considered together, while there is a constant frequency in the stator windings, a variable frequency will occur in the rotor bars according to the load. This variable frequency will cause differences in the inductance of the current flowing in the rotor bars and in the distribution of the current due to the skin effect. At this point, the geometrical shape of the rotor slots and therefore the rotor bars will cause significant effects on the speed-dependent torque performance.

At low speeds, high bar resistance will increase the starting torque. However, at high speeds, high bar resistance will negatively affect the efficiency. Short and wide rotor slots are the right choice for better starting torque and power factor, while deep and wide slots are advantageous in terms of efficiency[12].

Al cage is generally preferred as AFIM squirrel cage material as in conventional radial current induction motors. The primary reason for this preference is the cost and then the metallurgical properties of Al such as melting point and conductivity. Bars can be produced as fabricated Al or die-cast by using suitable moulds. With the progress in production technologies, die-cast cages have started to find more and wider use every day. In addition, although it is seen as a disadvantage in terms of cost, the use of Cu as a cage material has come back to the agenda due to the demand for high efficiency motors and increasing magnet costs[28]. Thanks to the Cu bars, 54% less losses due to squirrel cage can be achieved[29]. Figs. 4 to 9 shows the results of the FEM analysis of Cu and Al bars using different rotor slot geometries. CPU used in the analyses is Intel Core i5-6500HQ 3.2Ghz and the memory speed is 8 Gb RAM. TAU mesh method was used in the analyses. The number of elements in the mesh networks is 23,566 for Slot1. In the parametric analyses, the transient solution method was applied up to 0.1 s for each of the 99 steps. The time step was determined as 8e-5 s in the performed solutions.

The shape of Slot1 was determined by a slot geometry similar to the AURAGEN G8500 rotor slot, as it is a previously manufactured and tested DS-AFIM[23]. While determining the dimensions of this slot shape, basic dimensions were obtained according to 50 kW shaft power. According to the inner and outer diameter values obtained, the thinnest tooth thickness was determined as 3.32 mm in the stator. In the rotor, since the number of slots is more, the slot pitch is shorter. Accordingly, it is necessary to determine the width of the main body of the rotor slots narrower than the main body of the stator slots in order to prevent saturation in the rotor teeth. In the designs made, the rotor tooth width in the narrowest region in the 54 slot rotors was determined to be 3.73 mm. As mentioned before, the narrowest zone is formed at the inner diameter of the teeth.

In the slot design, designs were determined by considering the saturations in the cores. Torque, current, efficiency, power factor and shaft power, which are the determining parameters of motor performance,

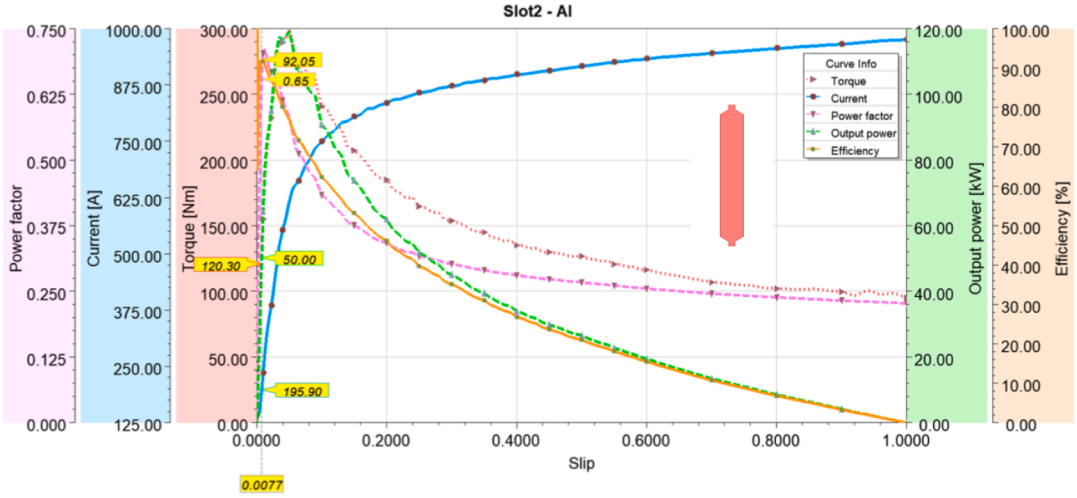

(a)

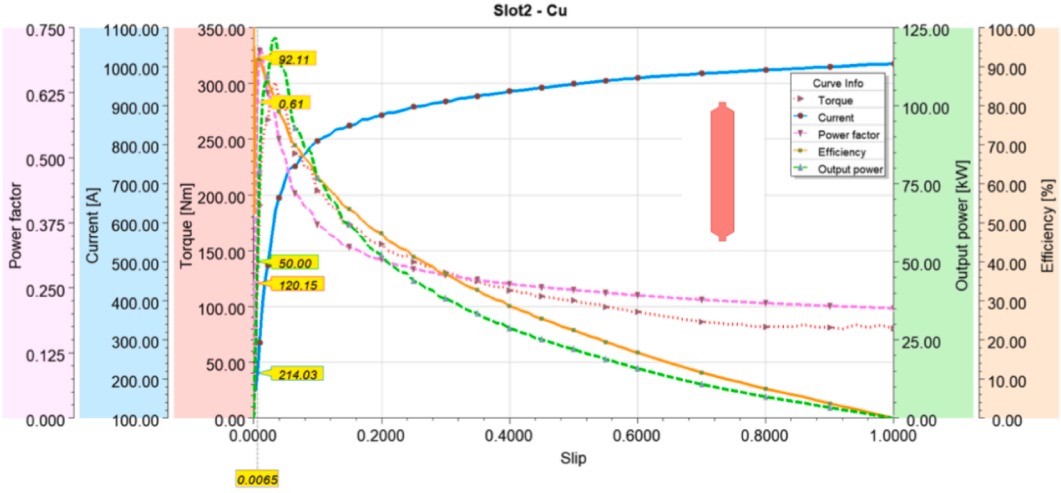

(b)

Fig. 5. Slot2 slip dependent performance curves.

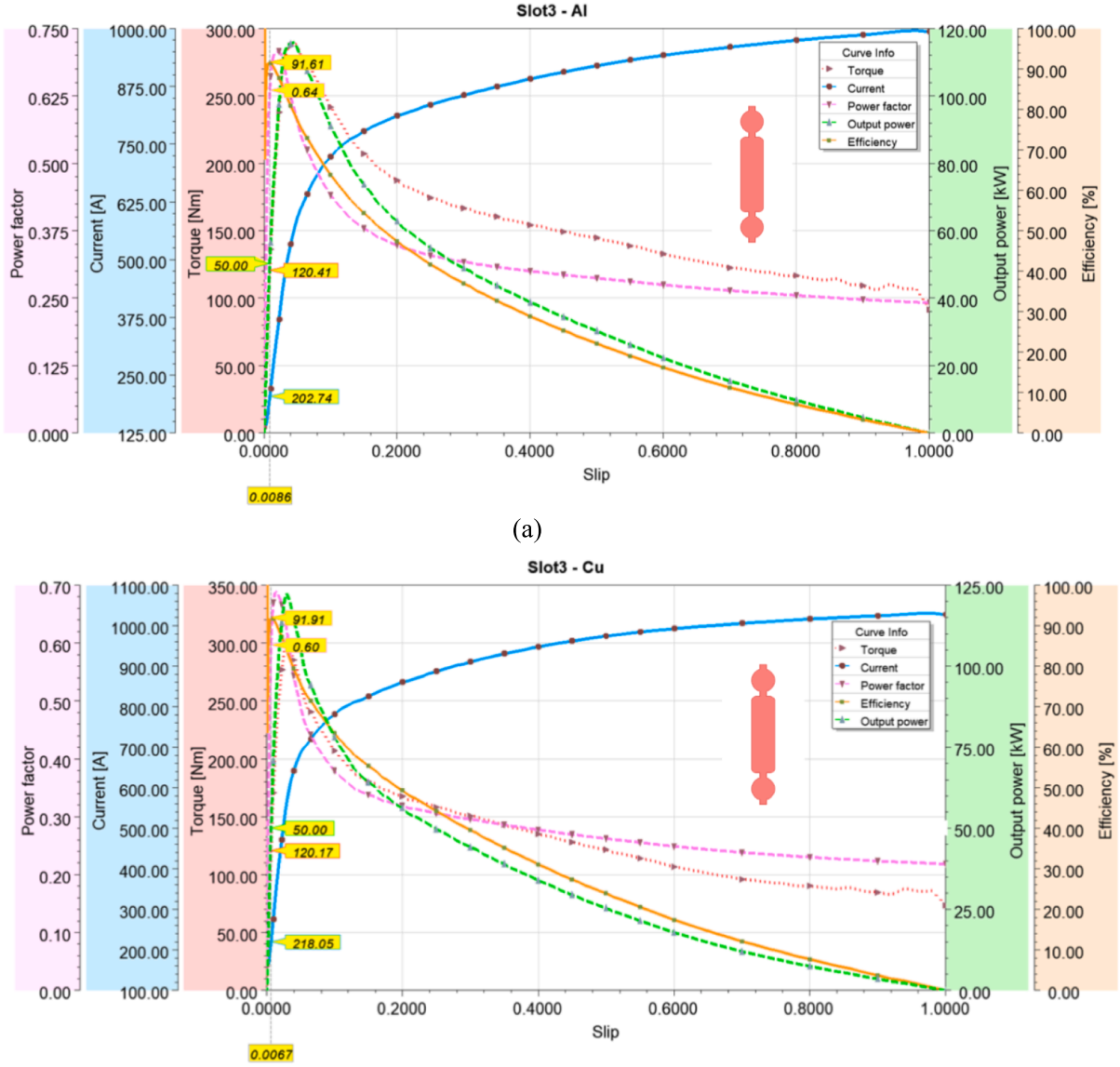

Fig. 6. Slot3 slip dependent performance curves.

were measured by FEM using parametric analysis. In the analyses, speed dependent results were evaluated as it is a good guide in determining the motor performance especially in variable speed applications. After dimensioning the rotor slot for each slot type, the rotor bar material was first determined as Al and then Cu and the analyses were repeated.

In Fig. 4, the performance graphs of the slot1 are presented. By looking at the torque graphs in Fig. 4(a) and Fig. 4(b), it is seen that the breakdown torque occurs at 3600 rpm in Al cage and 3700 rpm in Cu cage. The torque values at these speeds are obtained as 322.79 Nm and 323.67 Nm, respectively. The starting torques were measured as 114 Nm and 98.5 Nm for Al and Cu cage, respectively. At 50 kW output power, the performance data of each motor are shown on the graphs. Accordingly, the efficiency, power factor, torque and current values of the Al cage are 90.41%, 0.67, 121.38 Nm and 196.62A, respectively, when rotor slot1 is used at 50 kW output power. These values were measured as 92.12%, 0.67, 120.88 Nm, 196.05 A in Cu cage. Nominal power was reached at a speed of 3934 rpm in Al cage and 3950 rpm in Cu cage.

Fig. 5 shows the performance graphs of the slot2. In the torque graphs, the breakdown torque occurred at 3800 rpm for Al cage and occurred at 3860 rpm for Cu cage. The torque values at these speeds are 299.12 Nm for Al and 301.14 Nm for Cu. The starting torque is 94.9 Nm for Al cage and 80.41 Nm for Cu cage. At 50 kW output power, the efficiency, power factor, torque and current values are 92.05%, 0.65, 120.30 Nm and 195.9 A for Al cage at 3969 rpm. For Cu cage at 3974 rpm, these values are 92.11%, 0.61, 120.15 Nm and 214.03 A, respectively.

Fig. 6 shows the performance graphs of the rotor slot3. Accordingly, the breakdown torque obtained as 289.56 Nm at 3820 rpm for Al cage and obtained as 301.03 Nm at 3880 rpm for Cu cage. The starting torques were obtained as 91.5 Nm and 73.58 Nm for Al and Cu cages, respectively. The efficiency, power factor, torque and current values for the nominal power value obtained at 3966 rpm and 3973 rpm for Al and Cu are 91.61%, 0.64, 120.41Nm and 202.74 A for Al cage. These values are 91.91%, 0.6, 120.17 Nm and 218.05 A for Cu cage.

Fig. 7 shows the values of efficiency, power factor, torque, and current values of the rotor slot 4 depending on the slip. Accordingly, the breakdown torques were obtained as 300.94 Nm and 300.14 Nm at 3780 rpm and 3860 rpm for Al and Cu cages, respectively. The starting

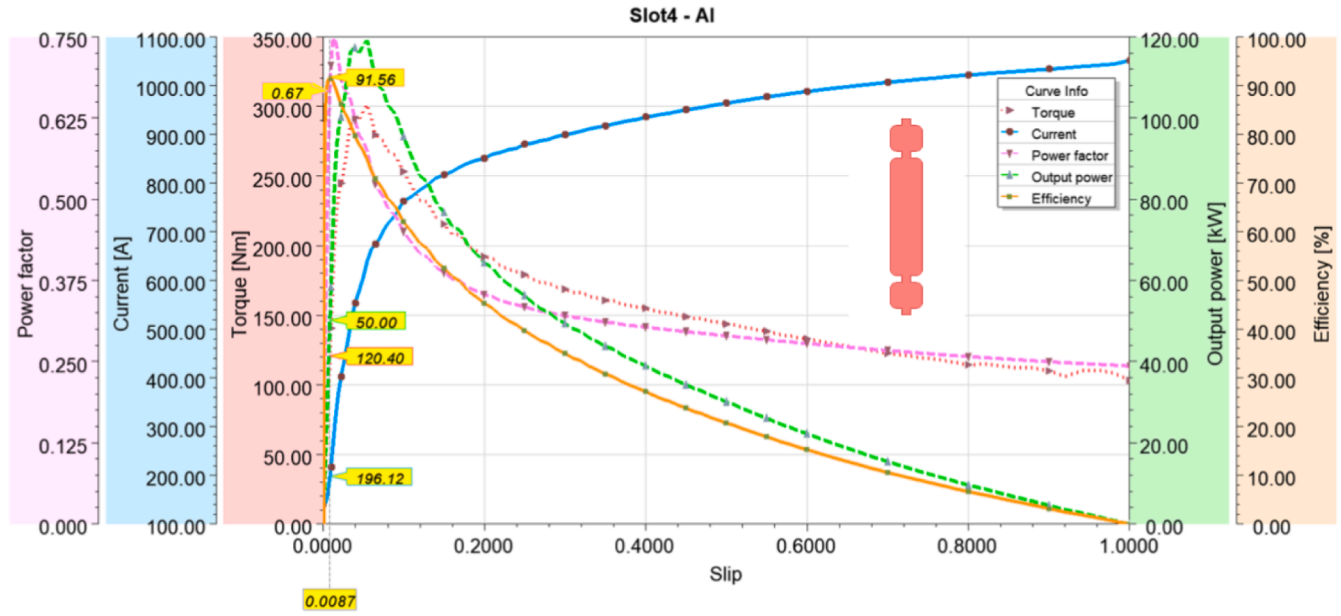

(a)

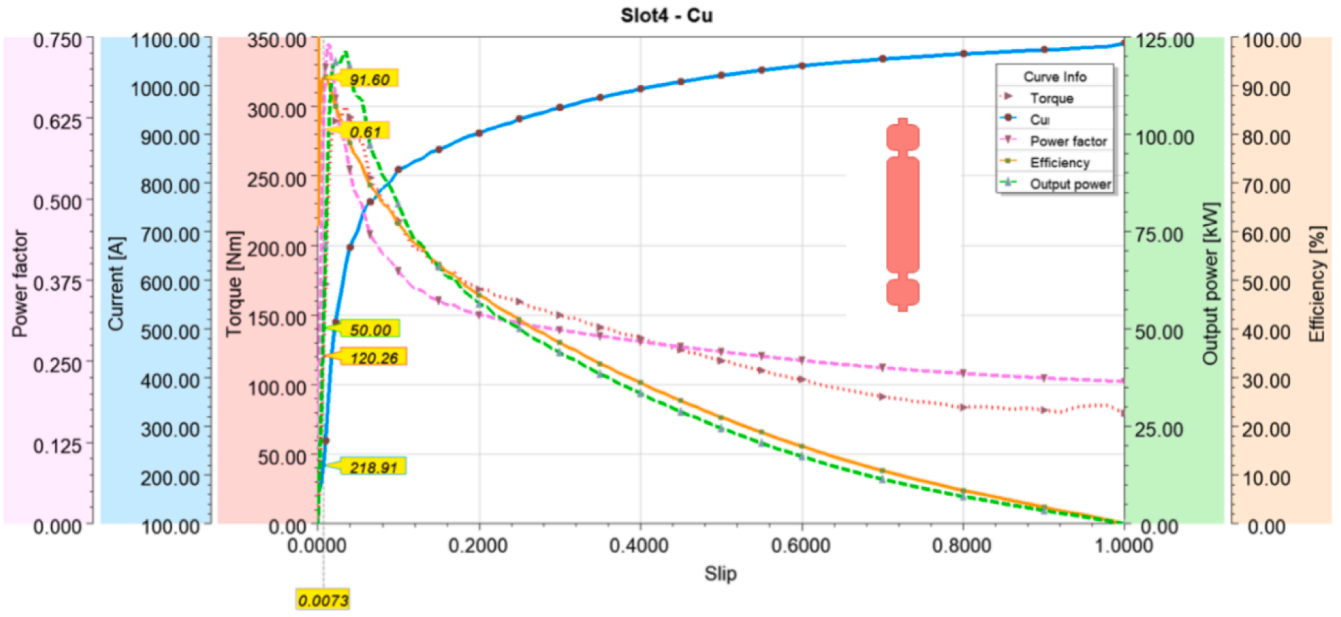

(b)

Fig. 7. Slot4 slip dependent performance curves.

torque is 103.1 Nm for Al cage and 79.41 Nm for Cu cage. 50 kW output power was achieved with 91.56% efficiency, 0.67 power factor, 120.4 Nm torque and 196.12A stator current at 3965 rpm in Al cage. In Cu cage, rated power was obtained with 91.60% efficiency, 0.61 power factor, 120.26 Nm torque and 218.91 A current at 3971 rpm.

Fig. 8 shows the performance graphs of the rotor slot5. According to graphs, 50 kW output power was obtained at 3961 rpm in Al cage. In Cu cage, this power was reached at 3971 rpm. At this power value for Al cage, the efficiency, power factor, torque and current values were 90.07%, 0.61, 120.53 Nm and 214.07 A, respectively. These data were obtained as 90.62%, 0.57, 120.24 and 232.37 A for Cu cage, respectively. Breakdown torques were obtained as 285.26 Nm and 301 Nm at 3840 rpm and 3890 rpm speeds for Al and Cu cages, respectively. The starting torques obtained for Al and Cu cage motors for slot5 are 135.9 Nm and 110.2 Nm, respectively.

Fig. 9 shows the performance graphs of the rotor slot6. Accordingly, the breakdown torque obtained as 314.82 Nm at 3780 rpm for Al cage and obtained as 332.77 Nm at 3860 rpm for Cu cage. The starting torques were obtained as 103.13 Nm and 77.20 Nm for Al and Cu cages, respectively. The efficiency, power factor, torque and current values for the rated power value obtained at 3957 rpm for Al cage are 90.75%, 0.67, 120.68Nm and 194.41 A for Al cage. These values are 91.79%, 0.64, 120.24 Nm and 205.76 A at 3970 rpm for Cu cage.

A summary of the values expressed graphically in Figs. 4 to 9 is given in Table 2. According to this, 50 kW nominal power can be obtained with the highest efficiency in Cu material cages. The highest power factor of 0.67 was obtained in Cu cages, except for the 1st slot, which was lower than Al alternatives. In addition, the nominal output power of the Cu cages was obtained at 4 to 13 rpm lower speed in all rotor slot types. When the double cage slots were analysed among each other, the

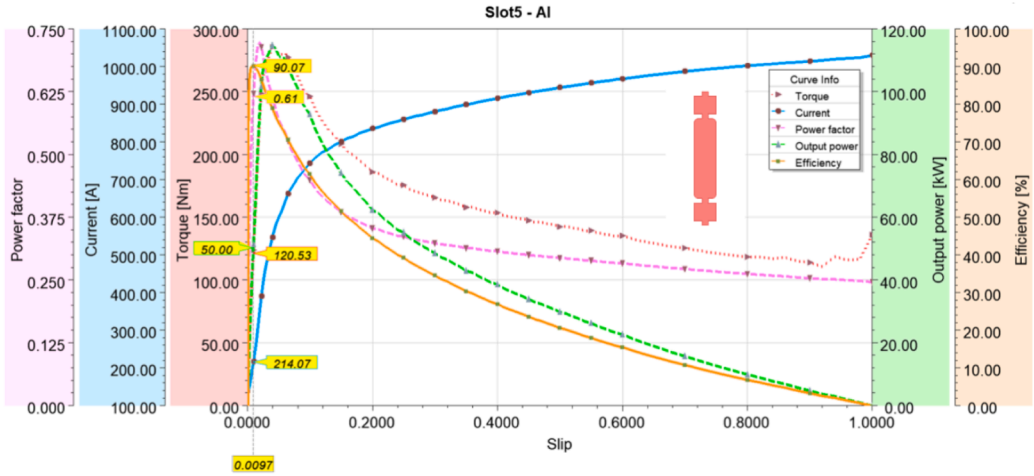

(a)

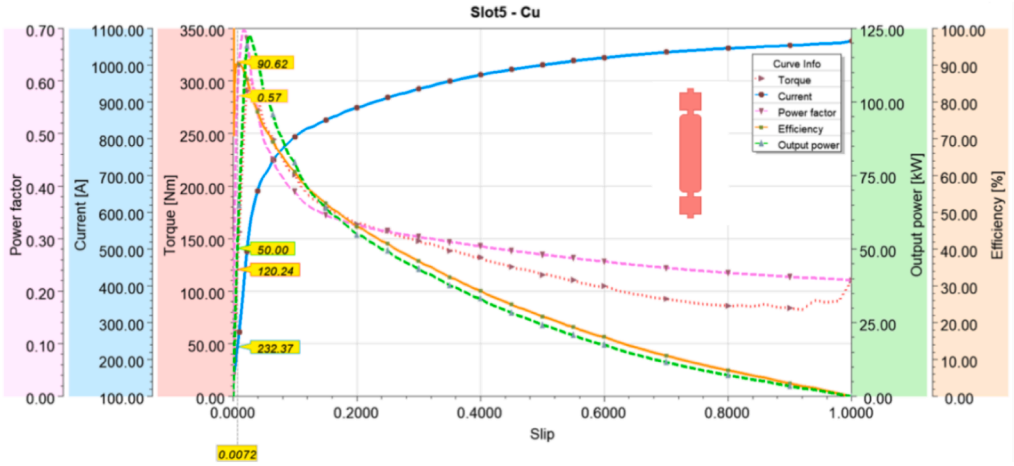

(b)

Fig. 8. Slot5 slip dependent performance curves.

difference in speed between Al and Cu became slightly more pronounced in the slots numbered 5 and 6, where the upper side of the slot has a corner. When the slots numbered 3, 4 and 5 were compared among themselves to examine the effect of the upper cage geometry of the slots, the highest efficiency was obtained in the Cu slot numbered 3, while the best power factor was obtained in the Al slot numbered 4 with 0.67.

It is more meaningful for motor design to evaluate performance measures such as efficiency and power factor together with current density in windings and flux density in cores. For this reason, Table 3 shows a summary of the current and flux density values of each slot type at 50 kW, 75 kW and 120 kW. Based on this, considering the core materials used in the stator and rotor, saturation will occur at flux densities higher than 2.1 T magnetic flux density. For the current density in the stator windings, a thermal failure will occur in the windings above the maximum value of 25 A/mm^2 with the liquid cooled stator jacket. Therefore, among all slot types, 120 kW output power can be obtained only when Cu cage is used in slot number 3. However, since the torque ripple at this level is 17%, it is not suitable for use in electric vehicles at this power level. In all slot options, 50 kW output power can be obtained according to the specified limit value. But, when 50 kW nominal and 75 kW maximum output power is desired to be obtained with a maximum ripple of 10% in order to be used as a traction motor in electric vehicles, the options are narrowed. The only option that can meet these constraints with both Al and Cu cage is rotor slot number 1. Slot number 4 can fulfill these constraints with only Al cage. Table 3 also shows the average flux density of the air gap at different power levels when Al and Cu cages are used in each slot geometry. This resulted in an average air gap magnetic flux density between 0.5771 T and 0.695 T.

Fig. 10 shows the comparison of the starting and nominal current and torque values of each rotor slot. If low current and high torque are a priority in the selection of the rotor slot geometry of the designed motor, Fig. 10 will provide preliminary information on this matter. Based on this, although the Cu cage slot geometries numbered 2 and 3 stand out in this regard, they are found to be unsuitable because they do not meet the other design criteria.

2D parametric FEM analyses of the rotor slot geometries were performed with ANSYS Electronics software using full models. According to the results of this analysis, the magnetic flux density on the rotor and stator cores at 50 kW nominal power and the distribution of flux lines on 1/6 models are expressed in Fig. 11. It is seen that there is no saturation in the motor parts, only negligible localized saturation in the tooth regions occured.

5. Conclusion

In this study, an 8-pole motor with a nominal power of 50 kW and a peak power of 75 kW is designed with different rotor slot geometries and different cage materials to be used as a traction motor in electric vehicles. 6 different rotor slot geometries are tested with FEM using both Al and Cu cages. 2D linear models of AFIMs were used in the analyses since they provide advantages in terms of analysis time and processor load. In order to reveal the effect of rotor slot shape and cage material on the

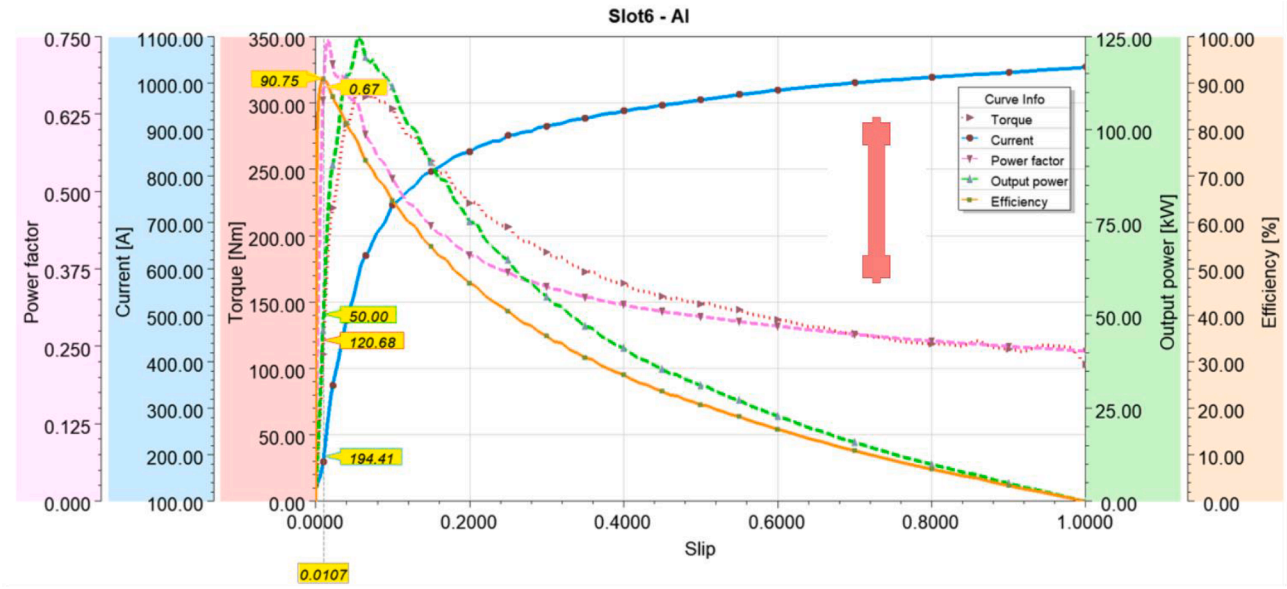

(a)

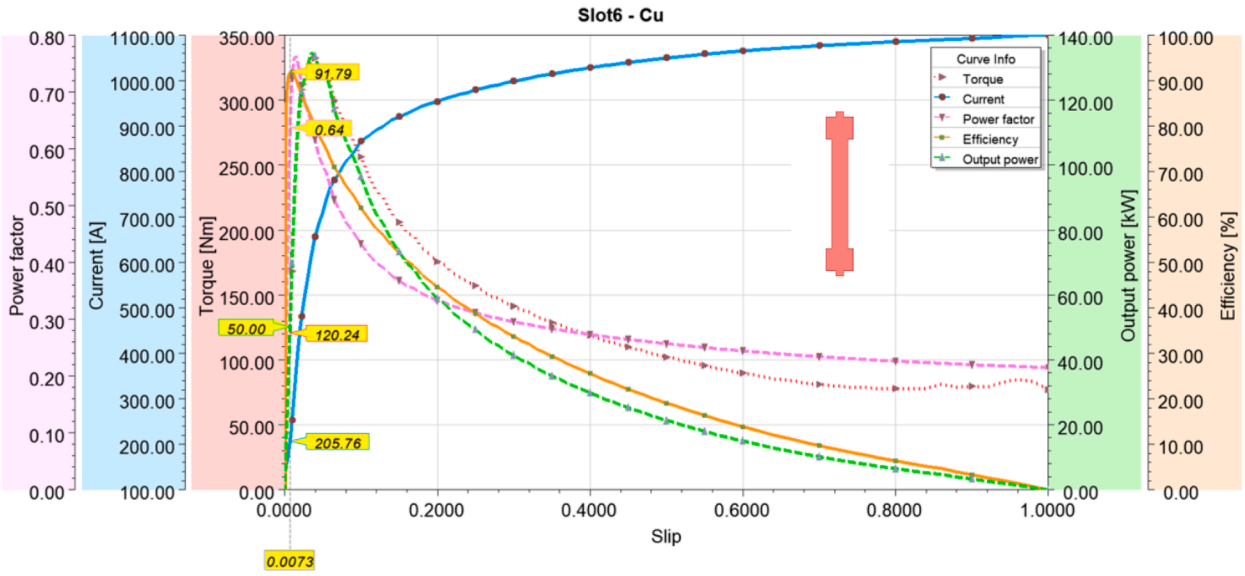

(b)

Fig. 9. Slot6 slip dependent performance curves.

Table 2
Motor performance parameters.

Rotor Slot Type / Cage Material	Speed (rpm)	Efficiency (%)	pf	Torque (Nm)	Current (A)
Slot1 / Al	3934	90.41	0.67	121.38	196.62
Slot1 / Cu	3950	92.12	0.67	120.88	196.05
Slot2 / Al	3969	92.05	0.65	120.30	195.90
Slot2 / Cu	3974	92.11	0.61	120.15	214.03
Slot3 / Al	3966	91.61	0.64	120.41	202.74
Slot3 / Cu	3973	91.91	0.60	120.17	218.05
Slot4 / Al	3965	91.56	0.67	120.40	196.12
Slot4 / Cu	3971	91.60	0.61	120.26	218.91
Slot5 / Al	3961	90.07	0.61	120.53	214.07
Slot5 / Cu	3971	90.62	0.57	120.24	232.37
Slot6 / Al	3957	90.75	0.67	120.68	194.41
Slot6 / Cu	3970	91.79	0.64	120.24	205.76

motor output parameters, the stator design was applied in the same way for all motors. In this way, 12 motors were analysed at 98 different speeds and slip-dependent performance graphs were obtained. As a result of the analysis, the highest efficiency at nominal operation was 92.12% when the rotor slot geometry number 1 with Cu cage was selected. In this motor, the current in the stator windings was measured as 196.05 Arms at 50 kW output power. A current density of 11.744 A/mm^2 was measured in the stator windings. This value was determined as a design constraint since the motor can reach up to 25 A/mm^2 current density by using the stator cooling jacket according to the determined design parameters. In addition, as another limiting factor, the maximum value of the magnetic flux density in the stator and rotor cores were set as 2.1 T. A maximum torque ripple of 10% is targeted to ensure smooth operation, which is among the important criteria in electric vehicles such as high efficiency and high thermal tolerance. According to these design criteria, for each rotor slot geometry and cage material, the maximum magnetic flux density in the stator teeth and the maximum current density in the windings were evaluated at power levels of 50 kW,

Table 3
Magnetic flux density and current density for different power levels.

		Output power (kW)	Stator tooth B_{max} (T)	Stator winding J_{max} (A/mm^2)	Rotor B_{max} (T)	Rotor bars J_{max} (A/mm^2)	Air gap average B_{avg} (T)	Tork ripple (%)
Slot 1	**Al**	50	1.9353	12.1512	1.5974	7.1415	0.6378	4.9501
		75	2.0657	16.596	1.5681	10.7538	0.6253	4.6797
		122	2.3504	34.5923	1.2073	26.0059	0.6195	3.6899
	Cu	50	1.8738	11.744	1.6075	6.6631	0.6388	5.7758
		75	2.071	16.6867	1.5727	10.7272	0.6253	4.4717
		122	2.3374	36.218	1.1773	27.7221	0.6185	4.4466
Slot 2	**Al**	50	1.994	11.9145	1.7475	9.5648	0.6266	10.6041
		75	2.1561	16.9679	1.9785	13.6918	0.6457	17.5189
		119	2.5149	37.9433	2.1326	47.5079	0.6949	29.2804
	Cu	50	1.9341	12.2535	1.7826	9.4387	0.6079	16.8961
		75	2.1904	15.8236	2.0133	16.751	0.5771	8.5708
		122	2.3967	37.2987	2.2445	59.3174	0.695	33.2838
Slot 3	**Al**	50	2.0745	9.9689	1.7518	8.9269	0.6393	17.0706
		75	2.1434	14.679	1.779	17.6224	0.6332	19.0345
		116	2.3992	28.0181	2.0166	30.7491	0.645	22.167
	Cu	50	2.0095	9.8229	1.8086	8.2986	0.625	14.0013
		75	2.1825	14.3615	1.811	18.7653	0.6237	20.8513
		125	2.3704	23.8245	2.0954	31.3248	0.6741	17.0595
Slot 4	**Al**	50	1.9466	10.5242	1.6689	7.8151	0.6324	8.5145
Slot 5		75	2.0667	12.8679	1.884	13.8868	0.661	6.5597
		119	2.3578	26.9268	2.229	34.2567	0.6469	26.6253
	Cu	50	2.0962	11.5201	1.9231	8.5003	0.6383	11.5755
		75	2.4575	31.4627	2.0943	49.2515	0.6437	26.6616
		121	2.4087	32.0494	2.103	40.3298	0.6522	26.6219
Slot 5	**Al**	50	2.097	10.6219	1.836	12.9833	0.6519	19.5637
		75	2.0854	15.3228	0.814	19.8549	0.6224	16.772
		115	2.4478	27.8966	2.0596	29.5352	0.6405	18.9449
	Cu	50	1.9386	10.5513	1.8313	11.7339	0.635	15.0984
		75	2.1707	17.8593	2.0551	23.805	0.6458	23.5898
		122	2.3728	27.0752	2.1144	33.7235	0.6276	40.3297
Slot 6	**Al**	50	1.8842	9.618	1.3349	10.0398	0.6415	15.9998
		75	2.0272	12.4118	1.6035	21.4854	0.626	13.5777
		125	2.3421	31.2747	1.5024	39.4789	0.6423	19.4112
	Cu	50	1.907	9.8367	1.4013	13.0427	0.6428	17.2224
		75	2.0697	14.9273	1.3466	18.4682	0.6422	15.2608
		135	2.4301	31.576	1.5415	51.0047	0.6167	24.9212

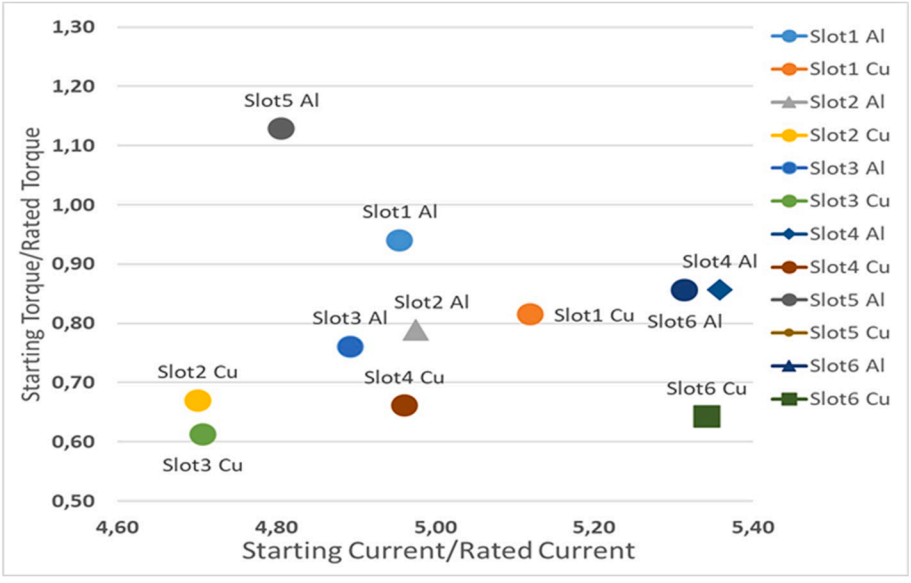

Fig. 10. Starting/rated torque and current ratios.

75 kW and at each alternating breakdown torque. In these evaluations, the max magnetic flux density in the rotor core, max current density in the rotor bars, air gap average flux density and torque ripple were analysed. The lowest torque ripple was obtained in slot number 1 at all power levels. At 50 kW and 75 kW output power, the torque ripple values in the slot number 1 were obtained as 4.9501%, 4.6797% for Al cage, and 5.7758%, 4.4717% for Cu cage, respectively. In these slot types and materials, as in all other alternatives, the design limit values at 120 kW level were exceeded in terms of both flux density and current density. In the rotor slot geometry number 1, which was determined as the most suitable option, higher efficiency was obtained with Cu cages compared to Al cages. When the results are considered as a complete set,

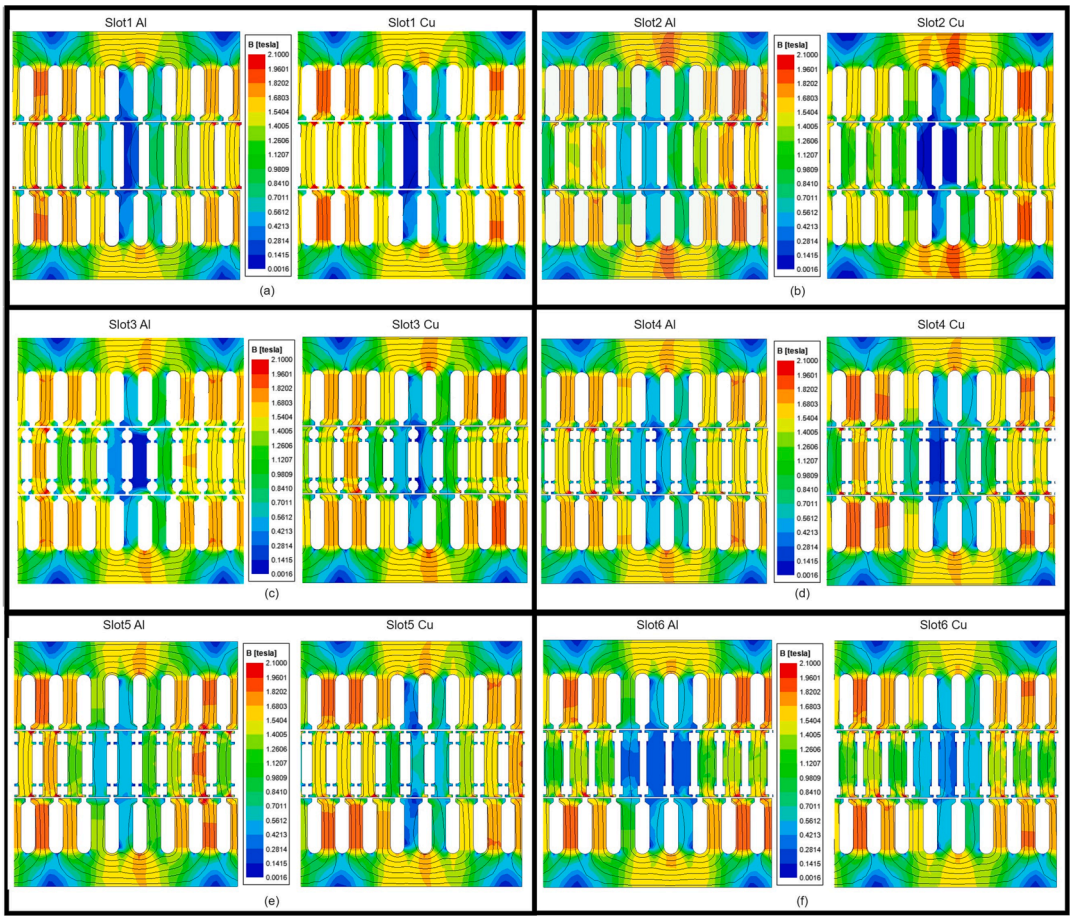

Fig 11. Magnetic flux densities on stator/rotor cores flux lines (a) Slot1 (b) Slot2 (c) Slot3 (d) Slot4 (e) Slot5 (f) Slot6.

high efficiency and low torque ripple, which are the main targets, have been achieved in the rotor geometry number 1 with Cu cage motor. In this study, the DS-AFIM 2D linear model was used to analyse different rotor slot geometries and cage materials. The study will contribute to researchers working in this field in terms of comparing different rotor slot geometries and cage materials in the use of AFIMs, which stand out as a magnetless motor, in electric vehicles. By applying the appropriate optimization method to the obtained results, it is possible to achieve higher efficiencies, especially by improving the pf value.

CRediT authorship contribution statement

Mustafa Özsoy: Investigation, Resources, Data curation, Visualization, Writing - original draft, Writing - review & editing. **Orhan Kaplan:** Conceptualization, Methodology, Validation, Supervision, Visualization. **Mehmet Akar:** Conceptualization, Methodology, Supervision, Project administration.

Declaration of Competing Interest

The authors declare that they have no known competing financial interests or personal relationships that could have appeared to influence the work reported in this paper.

References

[1] Dehghanzadeh AR, Behjat V, Banaei MR. Dynamic modeling of wind turbine based axial flux permanent magnetic synchronous generator connected to the grid with switch reduced converter. Ain Shams Eng J 2018;9:125–35. https://doi.org/10.1016/J.ASEJ.2015.11.002.

[2] Rodrigues Bruzinga G, Filho AJS, Pelizari A. Analysis and Design of 3 kW Axial Flux Permanent Magnet Synchronous Motor for Electric Car. IEEE Lat Am Trans 2022;20:855–63. https://doi.org/10.1109/TLA.2022.9693571.

[3] Wolnik T. Alternate computational method for induction disk motor based on 2D FEM model of cylindrical motor. Arch Elect Eng 2020;69:233–44. https://doi.org/10.24425/aee.2020.131770.

[4] Dianati B, Kahourzade S, Mahmoudi A. Optimization of Axial-Flux Induction Motors for the Application of Electric Vehicles Considering Driving Cycles. IEEE Trans Energy Convers 2020;35(3):1522–33. https://doi.org/10.1109/TEC.2020.2976625.

[5] Nobahari A, Darabi A, Hassannia A. Axial flux induction motor, design and evaluation of steady state modeling using equivalent circuit. 8th Power Electronics, Drive Systems and Technologies Conference, PEDSTC 2017 2017:353–8. https://doi.org/10.1109/PEDSTC.2017.7910351.

[6] Mei J, Lee CHT, Kirtley JL. Design of axial flux induction motor with reduced back iron for electric vehicles. IEEE Trans Veh Technol 2020;69:293–301. https://doi.org/10.1109/TVT.2019.2954084.

[7] Mahmoudi A, Ping HW, Rahim NA. A comparison between the TORUS and AFIR axial-flux permanent-magnet machine using finite element analysis. 2011 IEEE International Electric Machines and Drives Conference, IEMDC 2011 2011:242–7. https://doi.org/10.1109/IEMDC.2011.5994853.

[8] Nishanth FNU, Verdeghem J Van, Severson EL. Recent Advances in Analysis and Design of Axial Flux Permanent Magnet Electric Machines. 2021 IEEE Energy Conversion Congress and Exposition, ECCE 2021 - Proceedings 2021:3745–52. https://doi.org/10.1109/ECCE47101.2021.9595085.

[9] Selema A, Ibrahim MN, Vansompel H, Sergeant P. Development of Yokeless Axial Flux Machine Using 3D-Printed Shape-Profiled Core. 2022 International Conference on Electrical Machines, ICEM 2022 2022:1763–9. https://doi.org/10.1109/ICEM51905.2022.9910661.

[10] Bonnett AH, Albers T. Squirrel cage rotor options for A.C. induction motors. IEEE Conference Record of Annual Pulp and Paper Industry Technical Conference 2000:54–67. https://doi.org/10.1109/PAPCON.2000.854190.

[11] Williamson S, McClay CI. Optimization of the geometry of closed rotor slots for cage induction motors. IEEE Trans Ind Appl 1996;32:560–8. https://doi.org/10.1109/28.502167.

[12] Lordoglu A, Gulbahce MO, Kocabas DA. A comprehensive disturbing effect analysis of multi-sectional rotor slot geometry for induction machines in electrical vehicles. IEEE Access 2021;9:49590–600. https://doi.org/10.1109/ACCESS.2021.3068821.

[13] Junaid Akhtar M, Behera RK, Parida SK. Optimized rotor slot shape for squirrel cage induction motor in electric propulsion application. IEEE 6th India International Conference on Power Electronics (IICPE), vol. 2015- May, Kurukshetra,India: IEEE Computer Society; 2014, p. 1–5. https://doi.org/10.1109/IICPE.2014.7115846.
[14] Pao-La-Or P, Peaiyoung S, Kulworawanichpong T, Sujitjorn S. In: Effects of the Geometry of the Rotor Slots on the Mechanical Vibration of Three-phase Induction Motors. Beijing, China: Modelling and Optimization; 2007. p. 434–8.
[15] Yetgin AG, Durmuş B. Optimization of slot permeance coefficient with average differential evolution algorithm for maximum torque values by minimizing reactances in induction machines. Ain Shams Eng J 2021;12:2685–93. https://doi.org/10.1016/J.ASEJ.2021.01.012.
[16] Ghosh PK, Sadhu PK, Basak R, Sanyal A. Energy efficient design of three phase induction motor by water cycle algorithm. Ain Shams Eng J 2020;11:1139–47. https://doi.org/10.1016/J.ASEJ.2020.01.017.
[17] Joksimović G, Melecio JI, Tuohy PM, Djurović S. Towards the optimal 'slot combination' for steady-state torque ripple minimization: an eight-pole cage rotor induction motor case study. Electr Eng 2020;102:293–308. https://doi.org/10.1007/S00202-019-00874-X/TABLES/6.
[18] Cao Z, Mahmoudi A, Kahourzade S, Soong WL. An Overview of Axial-Flux Induction Machine. Proceedings of 2021 31st Australasian Universities Power Engineering Conference, AUPEC 2021 2021. https://doi.org/10.1109/AUPEC52110.2021.9597784.
[19] Egea A, Almandoz G, Poza J, Gonzalez A. Axial flux machines modelling with the combination of 2D FEM and analytic tools. 19th International Conference on Electrical Machines, ICEM 2010 2010. https://doi.org/10.1109/ICELMACH.2010.5608115.
[20] Madhavan R, Fernandes BG. A novel axial flux segmented SRM for electric vehicle application. 19th International Conference on Electrical Machines, ICEM 2010, Rome, Italy: 2010, p. 1–6. https://doi.org/10.1109/ICELMACH.2010.5608140.
[21] DIanati B, Kahourzade S, Mahmoudi A. Axial-flux induction motors for electric vehicles. 2019 IEEE Vehicle Power and Propulsion Conference, VPPC 2019 - Proceedings 2019. https://doi.org/10.1109/VPPC46532.2019.8952278.
[22] Corey C, Kim JH, Sarlioglu B. 2-D Modeling and Experimental Testing of Single Rotor Dual Stator Axial-Flux Permanent Magnet Machines. 2019 IEEE Energy Conversion Congress and Exposition, ECCE 2019 2019:2996–3003. https://doi.org/10.1109/ECCE.2019.8912517.
[23] Colombo L. Electromagnetic Sizing of Axial-Flux Induction Machines and Experimental Validation. 2021.
[24] Gundabattini E, Kuppan R, Solomon DG, Kalam A, Kothari DP, Abu BR. A review on methods of finding losses and cooling methods to increase efficiency of electric machines. Ain Shams Eng J 2021;12:497–505. https://doi.org/10.1016/J.ASEJ.2020.08.014.
[25] Ponomarev P. Tooth-coil permanent magnet synchronous machine design for special applications. 2013.
[26] Dorrell DG, Knight AM, Evans L, Popescu M. Analysis and design techniques applied to hybrid vehicle drive machines-assessment of alternative IPM and induction motor topologies. IEEE Trans Ind Electron 2012;59:3690–9. https://doi.org/10.1109/TIE.2011.2165460.
[27] Optimizing EV Traction Motor Performance from Concept Phase, Considering New Drive Cycles n.d. https://www.altair.com/newsroom/articles/Optimizing-EV-Traction-Motor-Performance-from-Concept-Phase-Considering-New-Drive-Cycles (accessed April 11, 2023).
[28] Finley WR, Hodowanec MM. Selection of copper versus aluminum rotors for induction motors. IEEE Trans Ind Appl 2001;37:1563–73. https://doi.org/10.1109/28.968162.
[29] Kirtley JL, Cowie JG, Brush EF, Peters DT, Kimmich R. Improving induction motor efficiency with die-cast copper rotor cages. 2007 IEEE Power Engineering Society General Meeting, PES, Tampa, FL, USA: 2007, p. 1–6. https://doi.org/10.1109/PES.2007.385767.

Mustafa Özsoy received his M.S. degree from Tokat Gaziosmanpasa University, Tokat, Turkey, in 2018. He is presently working towards his Ph.D. degree at Gazi University, Ankara, Turkey. He is also working as a Research Assistant at Tokat Gaziosmanpasa University. His current research interests include electric machines and electric vehicles.

Orhan Kaplan was born in Turkey. He graduated from the Department of Electrical Education of Gazi University in 2001. He received his M.Sc. and Ph.D. degrees from the Institute of Science & Technology, Gazi University in 2005 and in 2011 respectively. Dr. Orhan KAPLAN worked as a Research Assistant, Assistance Professor in Electrical Education Department at Gazi University. He became an Assoc. Prof. at Electrical & Electronics Engineering Dep. at Gazi University. Currently, he is working as an Assoc. Prof. at the same department. His main expertise field include power quality, electrical machines, renewable energy sources, microgrids, and smart grid applications. He served as reviewer to many high ranked scientific journals. He has published journal and conference papers on active power filters, reactive power compensation, sliding mode control, renewable energy sources, electrical machines, smart grid applications and industrial automation.

Mehmet Akar received the B.S. and Mc. S. degree in electrical education from Marmara University, Technical Education Faculty, Istanbul Turkey, and he received the Ph.D. degree in electronic and computer education from the University of Sakarya. He is currently working as a Professor at Tokat Gaziosmanpaşa University, Department of Electrical and Electronics Engineering. His research interests include electrical machines design, control and fault diagnosis.